tvst

Article

Macular Vascular Imaging and Connectivity Analysis Using High-Resolution Optical Coherence Tomography

Diogo Cabral[1,2], Ana C. Fradinho[2], Telmo Pereira[2], Meera S. Ramakrishnan[1], Tommaso Bacci[1], Dong An[3,4], Sandra Tenreiro[2], Miguel C. Seabra[2,5], Chandrakumar Balaratnasingam[3,4], and K. Bailey Freund[1,6]

[1] Vitreous Retina Macula Consultants of New York, NY, USA
[2] CEDOC, NOVA Medical School I Faculdade de Ciências Médicas, Universidade NOVA de Lisboa, Lisbon, Portugal
[3] Centre for Ophthalmology and Visual Science, University of Western Australia, Nedlands, Western Australia, Australia
[4] Lions Eye Institute, Nedlands, Western Australia, Australia
[5] UCL Institute of Ophthalmology, London, UK
[6] Department of Ophthalmology, NYU Grossman School of Medicine, New York, NY, USA

Correspondence: K. Bailey Freund, Vitreous Retina Macula Consultants of New York, 950 3rd Ave, 3rd Floor, New York, NY 10022, USA.
e-mail: kbfreund@gmail.com

Received: February 2, 2022
Accepted: May 6, 2022
Published: June 1, 2022

Keywords: high-resolution optical coherence tomography; macular blood flow; deep vascular complex

Citation: Cabral D, Fradinho AC, Pereira T, Ramakrishnan MS, Bacci T, An D, Tenreiro S, Seabra MC, Balaratnasingam C, Freund KB. Macular vascular imaging and connectivity analysis using high-resolution optical coherence tomography. Transl Vis Sci Technol. 2022;11(6):2, https://doi.org/10.1167/tvst.11.6.2

Purpose: To characterize macular blood flow connectivity in vivo using high-resolution optical coherence tomography (HighRes OCT).

Methods: Cross-sectional, observational study. Dense (6-µm interscan distance) perifoveal HighRes OCT raster scans were performed on healthy participants. To mitigate the limitations of projection-resolved OCT-angiography, flow and structural data were used to observe the vascular structures of the superficial vascular complex (SVC) and the deep vascular complex. Vascular segmentation and rendering were performed using Imaris 9.5 software. Inflow and outflow patterns were classified according to vascular diameter and branching order from superficial arteries and veins, respectively.

Results: Eight eyes from eight participants were included in this analysis, from which 422 inflow and 459 outflow connections were characterized. Arteries had direct arteriolar connections to the SVC (78%) and to the intermediate capillary plexus (ICP, 22%). Deep capillary plexus (DCP) inflow derived from small-diameter vessels succeeding ICP arterioles. The most prevalent outflow pathways coursed through superficial draining venules (74%). DCP draining venules ordinarily merged with ICP draining venules and drained independently of superficial venules in 21% of cases. The morphology of DCP draining venules in structural HighRes OCT is distinct from other vessels crossing the inner nuclear layer and can be used to identify superficial veins.

Conclusions: Vascular connectivity analysis supports a hybrid circuitry of blood flow within the human parafoveal macula.

Translational Relevance: Characterization of parafoveal macular blood flow connectivity in vivo using a precise segmentation of HighRes OCT is consistent with ground-truth microscopy studies and shows a hybrid circuitry.

Introduction

The inner retinal layers are vascularized by a capillary network with inflow from central retinal artery branches and drainage to central retinal vein tributaries.[1] The microcirculation in this network follows an intricate connectivity system that has neurophysiologic, optical, and metabolic particularities. A detailed understanding and the identification of normal morphologic patterns have important implications for the diagnosis and management of entities affecting the retinal vasculature.

Pioneering work on primate and human histology coupled with microscopic techniques identified up to four vascular networks in the perifoveal macula: radial peripapillary capillary plexus (RPCP), superficial vascular plexus (SVP), intermediate capillary

plexus (ICP), and the deep capillary plexus (DCP).[2–5] Recent technological advances in noninvasive imaging enabled the study of microvasculature in vivo in unprecedented detail. Employing projection-resolved optical coherence tomography–angiography (OCT-A) and structural optical coherence tomography (OCT), Campbell et al.[6] proposed a novel nomenclature with aggregation of the four plexuses into two vascular complexes with neurophysiologic and anatomic similarities: the superficial vascular complex (SVC), comprising the RPCP and SVP, and the deep vascular complex (DVC), composed of the ICP and DCP. The use of commercial OCT-A was further employed by many authors to evaluate macular microvasculature connectivity in vivo. Arguments in favor of predominantly in-parallel, in-series, or hybrid circuitry models were proposed to explain blood flow, which were supported by animal models[7–9] and structure–function relationships.[10–13]

While OCT-A was a breakthrough, technological limitations can confound a precise evaluation of macular connectivity, including projection artifacts, difficulties imaging flow coaxial to the scanning beam, and axial resolution (6–20 µm) greater than the mean retinal capillary diameter (8 µm).[14] These technology limitations and the absence of a volumetric ground-truth model may explain the lack of consensus in the connectivity models proposed.

Recently, An et al.[15] performed high-resolution confocal microscopy in perfusion-labeled human donor eyes, establishing a ground-truth model for connectivity analysis in the human macula. Their three-dimensional analysis demonstrated inflow to the DCP originating exclusively from the ICP and draining venules originating from each capillary plexus, supporting a hybrid model of macular connectivity, with both parallel and serial components. However, to the best of our knowledge, these findings have not been corroborated in vivo.

The high-resolution OCT (HighRes OCT) device, a recent development based on the SPECTRALIS multimodal imaging platform by Heidelberg Engineering (Heidelberg, Germany), increases the axial optical resolution of spectral domain OCT (SD-OCT) to 3 µm, which appears to enable more precise identification of retinal structures.[16] A previous study by Gattousi and Freund[17] demonstrated that there is sufficient contrast between vessels and surrounding structures in the middle retinal layers to observe the ICP and DCP using structural SD-OCT, thereby eliminating the limitations of OCT-A flow projection. Following this concept, we hypothesized that increased resolution and very dense structural acquisitions could enable imaging of the DVC and its interconnecting vessels with an enhanced signal-to-noise ratio, allowing us to trace the connections between the different plexuses in three-dimensional visualizations.

The aim of this work was to characterize macular blood flow connectivity in vivo using HighRes OCT.

Methods

Study Design and Setting

This was an observational study of healthy participants observed in December 2020 at Vitreous Retina and Macula Consultants of New York (New York, USA). This study was approved by the Western institutional review board and was conducted in accordance with the tenets of the Declaration of Helsinki (1964) and complied with the Health Insurance Portability and Accountability Act of 1996. All enrolled patients gave their written consent at the time of recruitment.

Participants and Image Acquisition

All participants were emmetropic, had no history of ocular or systemic diseases, and were not under any systemic drug treatment. The right eye of each participant underwent confocal true color fundus photography (CFP; EIDON AF, Centervue Padova, Italy) and HighRes OCT (structural and angiographic scans) based on the SPECTRALIS platform (Heidelberg Engineering). In OCT, the lateral optical resolution is decoupled from the axial optical resolution, which is determined by the coherence length (which is proportional to the central wavelength square and inversely proportional to the light source bandwidth).[18] The HighRes OCT instrument has an A-scan rate of 85 kHz and combines three superluminescent diodes to provide a center wavelength of 853 nm and a bandwidth of 137 nm (as compared to 880 nm and 45 nm, respectively, on the commercial SPECTRALIS device) to increase the optical axial resolution from approximately 7 µm to 3 µm in tissue, although its lateral optical resolution remains unchanged relative to the SPECTRALIS platform. The HighRes OCT uses the same auxiliary technologies as the SPECTRALIS, including TruTrack Active Eye Tracking, and Noise Reduction, which synergize to enhance OCT and OCT-A image quality and scan positioning accuracy. HighRes angiographic scans (HighRes OCT-A) consisted of 256 B-scans with a 6-µm interscan distance. Seven repeated OCT B-scans at each tissue location were used by the full-spectrum probabilistic OCT-A algorithm to determine the presence or absence of flow at each voxel. Scanning patterns measuring 10 × 5 degrees targeted the superior, inferior, and temporal perifoveal region.

Dense (6-µm interscan distance) structural raster scans with 30 frames averaged per B-scan were done subsequently using a pattern measuring 15 × 10 degrees that encompassed the regions scanned by HighRes OCT-A.

Investigational versions of Heidelberg Eye Explorer (Heidelberg Engineering) were used: version 6.12.4.710 for registration of HighRes OCT with external images and version 6.16.100.701 for acquisition, analysis, processing, and postprocessing of data. Multilayer segmentation was applied using the manufacturer's algorithms, and raw (floating point) data were exported as .VOL files for further analysis.

Image Analysis

The input for image analysis was the raw data (flow and structure) obtained from HighRes OCT-A acquisition. Image processing was done separately in the flow and structural volumes to highlight the retinal vasculature. To process the flow volume, a projection artifact removal[19] method was employed, followed by contrast-limited adaptive histogram equalization (CLAHE) using MATLAB (MathWorks, Natick, MA, USA) function *adapthisteq*, two-dimensional Gaussian filtering ($\Sigma = 0.7$), and Kalman filtering (prediction bias = 0.50; system noise estimate = 0.50).[20] To process the structural volume, a compensation operator for light attenuation was applied to diminish the artifacts created from blood vessel shadows.[21] Then, a denoising algorithm (block matching and three-dimensional filtering)[22] was applied to reduce speckle noise. Finally, two inbuilt MATLAB functions were used to perform morphologic (*imtophat*) and orthogonal (*pca* [principal component analysis]) transformations. Subsequently, CLAHE, two-dimensional Gaussian filtering ($\Sigma = 0.7$), and Kalman filtering (prediction bias = 0.50; system noise estimate = 0.50)[20] were employed. The output of the herein described image processing included two volumes (flow derived and structure derived) with enhancement of the retinal vasculature. These volumes were fused using different weighted contributions in the construction of the SVP and DVC. Since reduced contrast between vessels and surrounding tissue in the SVP limits the utility of structural OCT to analyze vessel connectivity in the more superficial retinal layers, flow signal data were used to analyze vessel connectivity in the SVP. As such, flow-derived volume accounted for 100% of the data in the SVP, and structure-derived volume accounted for 80% of the data in the DVC. The final output of the image analysis was a volume of the inner retina vascular network. The different processing steps are illustrated in Supplementary Figure S1.

Classification of Vascular Networks and Retinal Vessels

The scans were manually checked for correct segmentation of the inner limiting membrane (ILM), the ganglion cell layer (GCL), the inner plexiform layer (IPL), the inner nuclear layer (INL), and the outer plexiform layer (OPL). Vascular complexes were segmented as previously described.[6,13,23] The SVC was defined as including the nerve fiber layer, GCL, and inner aspect of the IPL, as previously described.[6,23] Automated segmentation parameters included the ILM and a 17-μm offset anterior to the IPL (IPL (–)). The DVC was defined as bracketing the outer aspect of the relatively thin IPL, INL, and the synaptic portion of the OPL.[6,13] Automated segmentation parameters included IPL (–) and the OPL boundary (OPL).

Confocal CFPs were registered with HighRes OCT using the plugin "landmark correspondences" of Fiji (ImageJ v1.52p; National Institutes of Health, Bethesda, MD, USA),[24] with the color images considered the gold standard to distinguish arteries from veins in the corresponding HighRes OCT volumes.[25] Retinal blood vessel type, as defined by Hogan and Feeney[26,27] and adopted by An et al.,[15] were used to classify vessels. As such, arteries were defined as SVC vascular structures with a diameter >15 µm and a location in CFPs matching retinal arteries. Veins were defined as SVC vascular structures with a diameter >20 µm and a location in CFPs matching retinal veins. Arterioles were defined as vascular structures branching from arteries with a diameter <15 µm and venules defined as vascular structures connecting to veins or other venules with a diameter <20 µm. Capillaries were defined as structures with a diameter <8 µm.

Volume Rendering and Rendering Quality Assessment

The volume of the inner retina vascular network was imported into Imaris v9.5 (Bitplane; Andor Technology plc., Zurich, Switzerland), and its built-in algorithms were used for vascular segmentation and three-dimensional analysis. The filament tracer module was used to obtain a replica of the superficial vessels, as previously described.[28] Superficial vessels were segmented automatically using the Imaris built-in algorithm *threshold loops*. The following parameters were introduced in this step: preprocessing of 20 µm and branch length to trunk ratio of 10. The remaining vessels were segmented semiautomatically by one investigator applying the following protocol. Branching points of superficial vessels were selected as starting points, the subsequent bifurcation on the volume was

selected, and the Autopath function was applied to automatically draw the path between them based on signal strength. Consequently, the Autopath algorithm necessitates a continuous vascular signal between the two selected points. This process was operated until all continuous vascular signal was segmented. To help follow vascular connectivity, SVC vessels were false-colored bright red/blue and the ICP false-colored dark red/blue, according to proximity to arterial and venous connections, respectively. The DCP was false-colored very dark blue.

Quality assessment was performed to validate the output of the image processing for HighRes OCT images. Ground-truth data were obtained after OCT-A manual segmentation of retinal capillaries by an observer who did not have access to the image-processing output. Bidimensional en face projections of the image-processing output spanning ICP and DCP boundaries were performed to observe the intermediate and deep capillary plexuses, respectively. These slabs were binarized, skeletonized, and dilated to obtain filament data. We determined the algorithm's accuracy based on the spatial overlap of the resultant data sets (ground-truth and filament data), that is, the total number of correctly classified pixels as a fraction of and the number of pixels present in the field of view. The process for evaluating rendering quality is depicted in Supplementary Figure S2.

Evaluation of Connectivity Pathways

The Imaris three-dimensional viewer was used to visualize the retinal vasculature at different angles of rotation. For inflow analysis, branches of superficial retinal arteries meeting arteriole definition were followed until reaching a capillary level. Likewise, for outflow analysis, branches from the superficial retinal veins corresponding to venule definition were tracked. We further evaluated how capillaries from each vascular plexus converged into venules and looked for the presence of vessels between plexuses. Morphologic patterns were identified and their prevalence quantified in five parafoveal areas of 1 mm^3 per eye (superior, super-temporal, inferior, inferotemporal, and temporal). We did not evaluate nasal areas to avoid the potential implications of a cilioretinal artery and the RPCP in our analysis.

Characterization of Deep Vascular Complex Interconnecting Vessels

The hyperreflective OCT band corresponding to the INL was inspected in structural HighRes OCT raster scans to detect vessels connecting the ICP and the DCP. When connecting vessels were identified, the display was set to 1:1 pixel to micrometer scaling before measuring vascular diameter with the HighRes OCT software caliper tool. Registered en face views of the DCP were used to localize the origin of connecting vessels, and three-dimensional visualization was conducted to analyze their connections with other vessels within the volume rendering of the image-processing output.

Results

General Characteristics

The right eyes from four male and four female participants were evaluated. The mean ± standard deviation age of the participants was 28 ± 4 years. In 422 inflow and 459 outflow connections, a mean number of 9 ± 3 inflow and 10 ± 3 outflow pathways per square millimeter was observed. With HighRes structural OCT, 146 interplexus connections in the DVC were identified. The accuracy (overlap percentage) between image-processing output and ground-truth manual segmentation was 78% ± 4% and 75% ± 5% for the ICP and the DCP, respectively.

Inflow Analysis

Inflow patterns and arrangement are depicted in Figure 1. Two patterns of arteriolar branches from superficial arteries were observed: a connection with the SVC (78% of the branches) and a connection with the ICP (22% of branches), that is, for each four arterioles supplying the SVC, there was one supplying the ICP. The proportion of inflow patterns was similar among the parafoveal areas evaluated ($P = 0.20$). The SVC was arranged as a network of capillaries branching from arterioles with small-diameter connections (<10 µm) between the SVC capillary network and the ICP (Fig. 1A). The ICP was arranged as a network of capillaries connecting with the other vascular plexuses (Fig. 1B). The sole source of DCP inflow was ICP small-diameter vessels that followed a spiral shape (Figs. 1C, 1D).

Outflow Analysis

The most prevalent outflow patterns that accounted for 96% of the observations are depicted in Figure 2. Venous outflow patterns were categorized by the organization of connections occurring in the

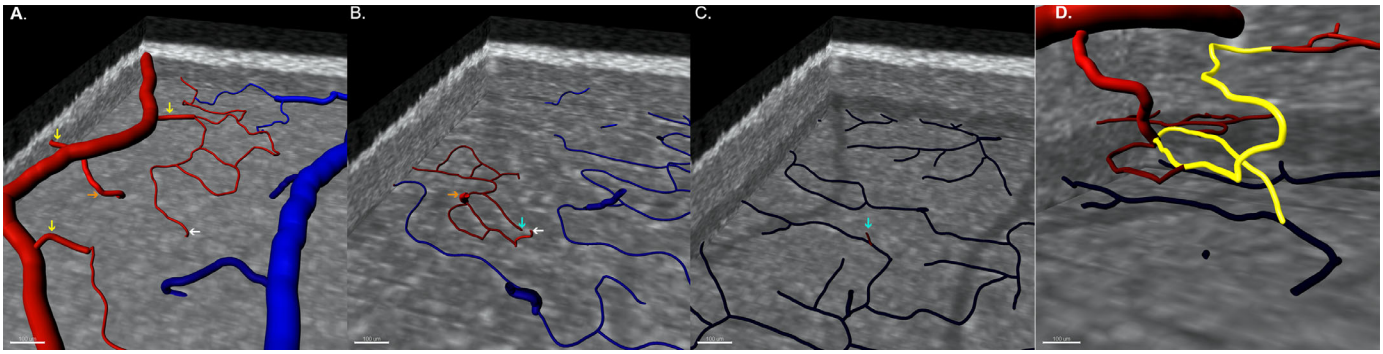

Figure 1. Three-dimensional observation of inflow vascular patterns. Superior views of the parafoveal vascular plexuses (A–C) enable precise tracing of inflow pathways (*arrows*) within a three-dimensional network. Vascular segmentation is color-coded according to connections to the superficial artery (*red*) or vein (*blue*). (A) Visualization of the SVC shows large-diameter connections to the SVC (*yellow arrows*) and to the ICP (*orange arrow*). A small-diameter vessel connecting the SVC capillary network to the ICP is indicated by a *white arrow*. (B) Visualization of the ICP demonstrates inflow from large (*orange*) and small (*white*) diameter vessels. (C) Visualization of the DCP demonstrates that the inflow comes from small-diameter vessels departing from the ICP in the vicinity of inflow from the superficial artery (*cyan arrow*). (D) Three-dimensional visualization of the ensemble of small-diameter inflow connections (*yellow pathway*) shows a spiral shape.

lower-order vessels prior to venule drainage into the larger superficial veins. The most common pattern (type 1, 75%) were superficial venules that had received smaller-size vessels from the SVC. Of these type 1 venules, 34% received drainage exclusively from SVC capillaries (type 1A), 30% received drainage exclusively from the ICP (type 1B), and 13% received drainage from both the DCP and ICP (type 1C). The second

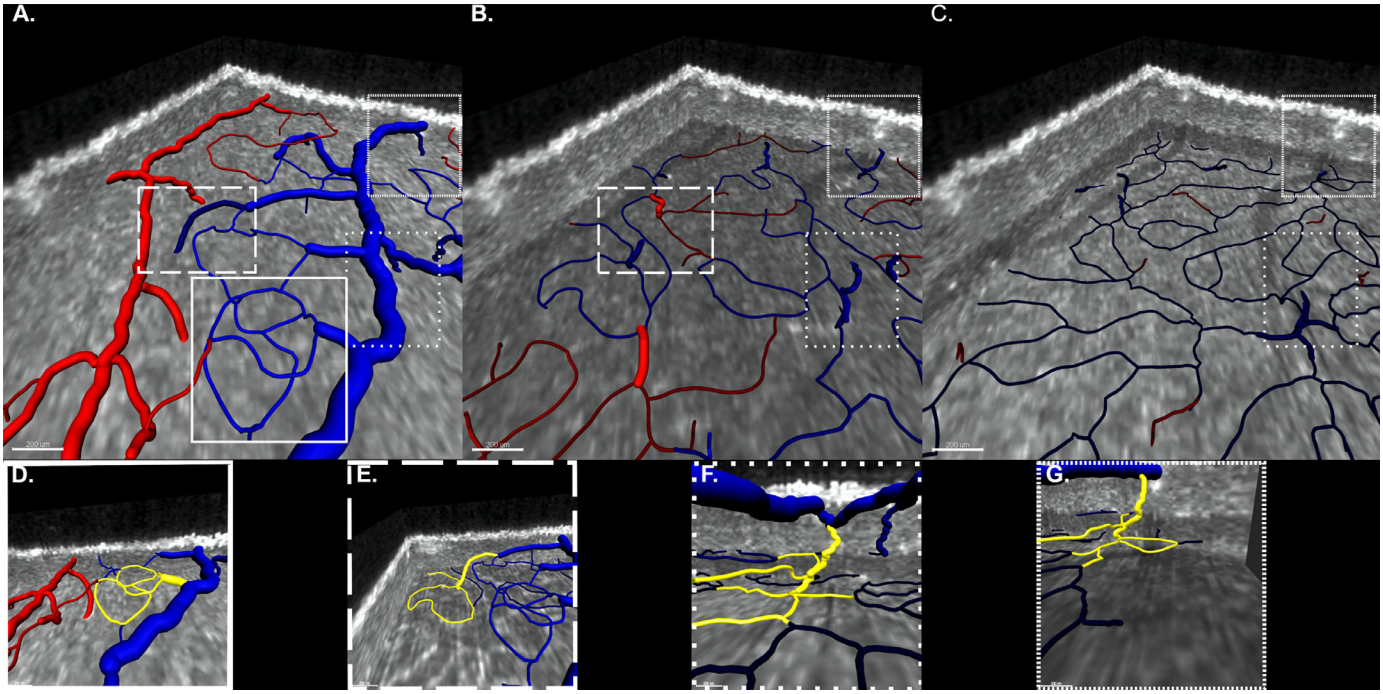

Figure 2. Three-dimensional observation of outflow vascular patterns. (*Upper row*) Superior views of the parafoveal vascular plexuses (A, SVC; B, ICP; and C, DCP) enable tracing of outflow pathway connections. Vascular segmentation is color-coded according to connections to the superficial artery (*red*) or vein (*blue*). Outflow pathways are classified according to the venule connecting to the superficial vein and its afferent connections. Each pathway is bounded by a specific *dashed line* to help follow the course and connections of each draining venule within the volume. (*Lower row*) Three-dimensional visualizations highlighting the morphologic features of each outflow pattern (D–G). (D) Type 1A outflow pattern (32%): draining venule receiving connections from the SVC. (E) Type 1B outflow pattern (30%): draining venule receiving connections from the SVC and a venule draining the ICP. (F) Type 1C outflow pattern (13%): draining venule receiving connections from the SVC and a venule draining the ICP and the DCP. (G) Type 2 outflow pattern (21%): a venule draining both the ICP and the DCP abuts directly in the superficial vein. These four patterns represent the large majority (96%) of the outflow patterns observed.

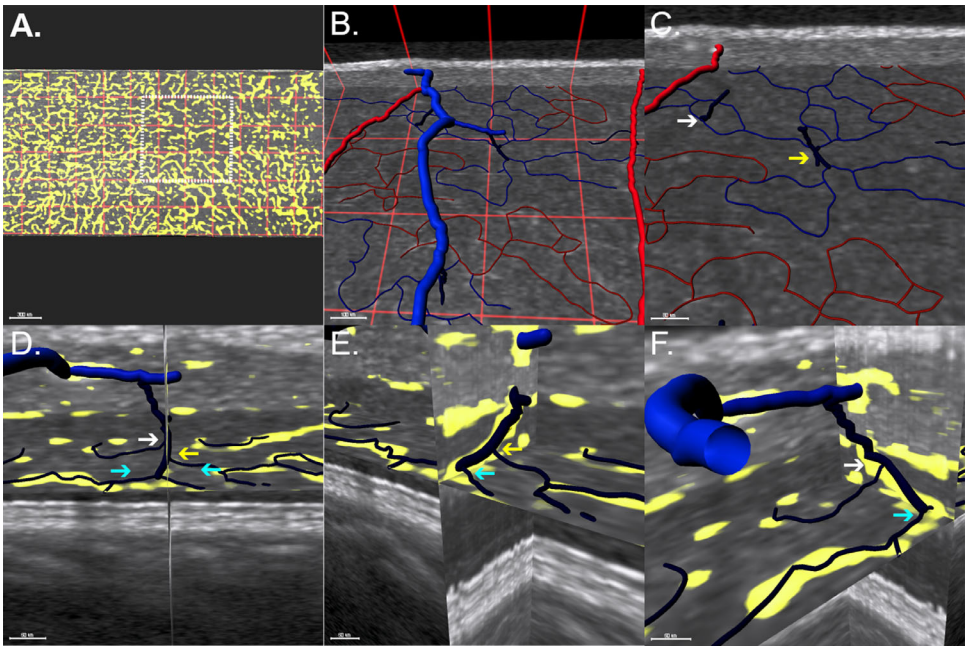

Figure 3. Morphologic characteristics of deep vascular complex outflow pathways. (A) En face view of the ICP. The image is divided by a *red grid* comprising squares sized 330 × 330 µm. A *white dashed square* highlights the region shown in B and C. (B) Superior view includes superficial larger vessels with ICP and ICP draining venules. (C) Magnified view showing two distinct configurations of capillary convergence. The *white arrow* indicates the convergence of two capillaries draining a small region, and the *yellow arrow* indicates a draining venule resulting from the convergence of four capillaries. (D) Coronal view of a venule originating from a DCP vortex. A plane spanning the XY axis is centered on the venule. (E, F) Orthogonal views demonstrate that DCP capillaries join the draining venule at different levels on the XY plane (*different-colored arrows*), resembling a spiral staircase morphology.

most common pattern (type 2, 21%) were draining venules originating in the DVC from convergence of DCP capillaries and additional drainage connections within the ICP. Less common patterns were venules originating in either the ICP (type 3, 3%) or the DCP (type 4, 1%), which received no additional connections prior their connection to a superficial vein.

The morphology of ICP and DCP outflow patterns is depicted in Figure 3. Most ICP venules (80%) resulted from the convergence of two ICP capillaries, while the remaining ICP venules originated from three or more ICP capillaries converging. The DCP venules showed a vortex morphology, best seen with an en face view; however, three-dimensional study demonstrated

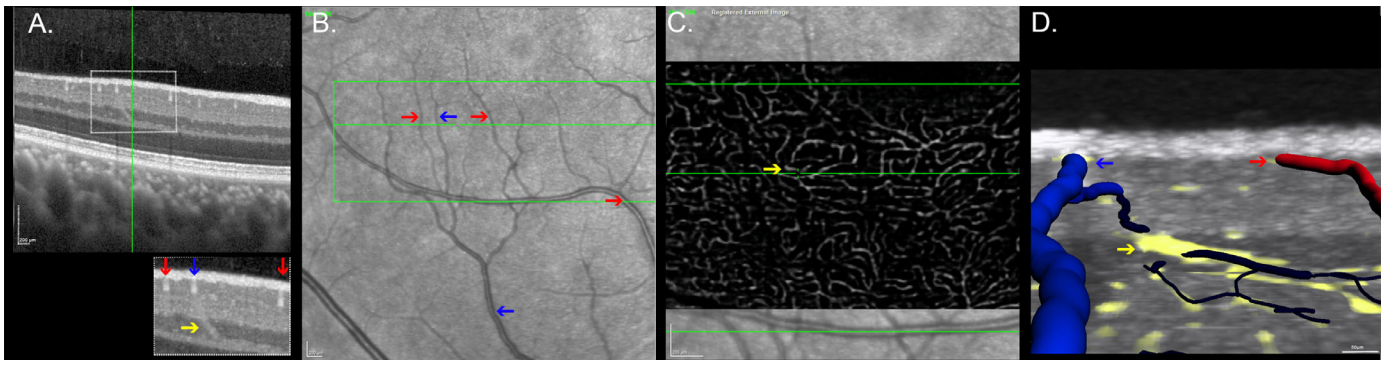

Figure 4. Correspondence between structural and angiographic HighRes OCT scans of the deep capillary plexus draining venules. (A) HighRes OCT B-scan of the inferotemporal parafoveal region. The *inset* highlights an oblique vessel (*yellow arrow*) crossing the inner nuclear layer. Superficial plexus vessels are labeled as veins (*blue arrows*) and arteries (*red arrows*) in the registered near-infrared reflectance image (B). (C) An en face view of the DCP registered with structural HighRes OCT demonstrates the origin of the vessel at the convergence of several DCP capillary size vessels (DCP vortex). (D) Three-dimensional visualization shows a course between the DCP (*dark blue*) and an SVC venule (*light blue*), supporting that this vessel is a DCP draining venule.

that within this vortex arrangement, DCP capillaries joined draining venules at slightly different levels of the z axis, resembling a staircase arrangement.

DVC Connecting Vessels Analysis

Multiple interplexus vessels connecting and DCP and ICP were identified. However, only the larger of these with a diameter of 20.5 ± 2.5 µm were amenable to detailed measurements. These larger vessels traversed the combined INL/Henle's fiber layer with a vertical or oblique orientation angled toward their target superficial vein. Registration with en face images of the DCP and three-dimensional visualization demonstrated these vessels to all be draining venules originating from the DCP vortexes. Figure 4 displays DCP draining venules identification and characteristics in OCT B-scans.

Discussion

In this study, we employed a novel approach to assess macular vasculature connectivity in vivo by combining vascular imaging from averaged structural HighRes OCT with HighRes OCT-A and applying three-dimensional reconstruction to trace vascular connections. We demonstrated the feasibility of using structural HighRes OCT images for detailed visualization of the DVC through an analysis of 422 inflow and 459 outflow pathways. Inflow analysis revealed that superficial arteries have large arteriolar connections exclusively supplying the SVC and ICP and that the DCP inflow derives from small vessels that originate from ICP arterioles. Outflow analysis demonstrated the convergence of capillaries to draining venules in every plexus and DCP draining venules ordinarily receiving ICP drainage. We also identified imaging features of DCP draining venules in structural OCT images that enable the identification of venous confluence areas and superficial veins. Our findings show a better correspondence with ex vivo high-resolution confocal microscopy imaging of retinal vasculature compared to previous studies reporting alternative connectivity patterns below the SVC.[6,29] Our observations also support a hybrid model of flow between arteries and veins in the human perifovea, with a parallel circuit in the SVC and ICP, as well as an in-series circuit through the DCP. Figure 5 represents a schematic representation of the parafoveal connectivity according to the predominant inflow and outflow patterns observed.

The use of dense volumes of highly averaged structural OCT B-scans to observe DVC capillary plexuses was first conceptualized by Gattousi and Freund.[17]

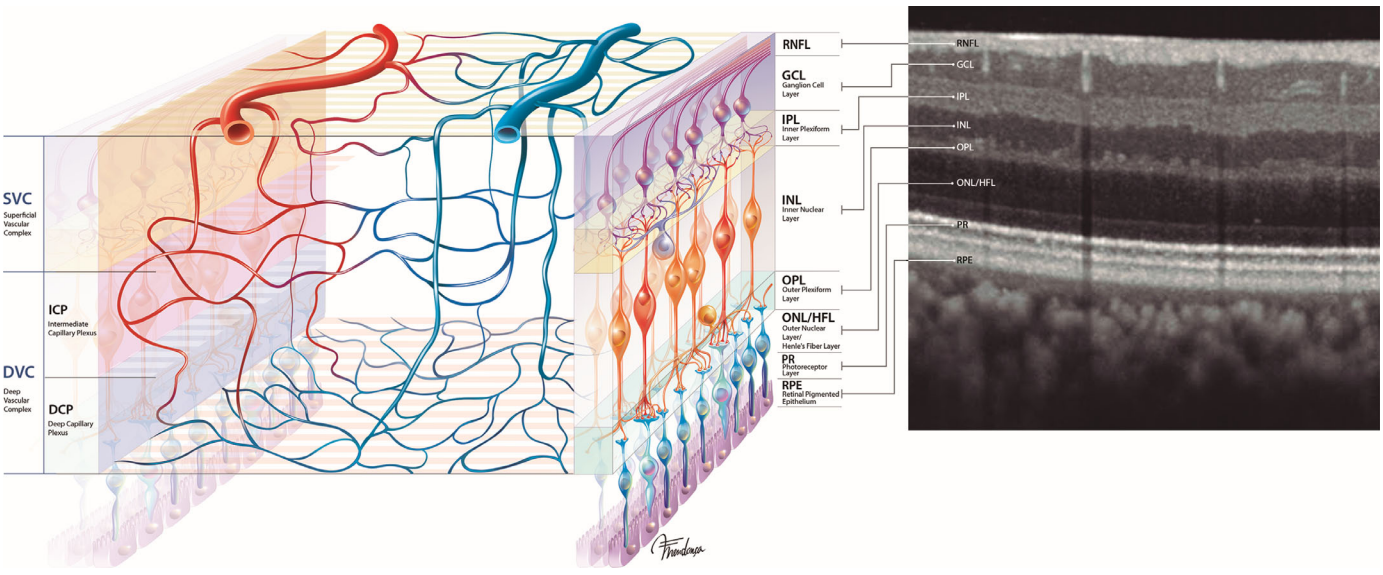

Figure 5. Schematic representation of the parafoveal vascular network demonstrating the most frequently observed connectivity patterns observed with HighRes OCT. Superficial arteries supply the network through large arteriolar connections to the SVC and ICP. DCP inflow derives from small vessels succeeding ICP arterioles. Venules originate from the convergence of capillaries in every plexus. SVC draining venule is the venule that abuts most frequently the superficial vein and often receives venules from the plexuses below. DCP draining venules angle toward a superficial vein and typically receive ICP draining venules prior to reaching this target. The schematic representation demonstrates a hybrid model of flow between arteries and veins in the human parafovea, with a parallel circuit in the SVC and ICP and an in-series circuit through the DCP.

The authors demonstrated that differences in reflectivity can be used to observe the DVC plexuses using en face OCT and a precise anatomic segmentation to mitigate the limitations of projection-resolved OCT-A. In this work, we built on this concept and applied it to HighRes OCT technology. The comparison between our approach and manual segmentation of blood vessels in OCT-A scans demonstrated parity to an expert user. However, reduced contrast between vessels and surrounding tissue in the SVC limits the utility of using structural OCT to analyze vessel connectivity in the more superficial retinal layers. Therefore, we used HighRes OCT-A flow signal data to analyze vessel connectivity in the SVC. Three-dimensional analysis of the combined structural and flow data demonstrated an average number of pathways per square millimeter closely corresponding with the value observed in ground-truth microscopy analysis.[15]

Consistent with previous histology[2,5] and OCT-A studies,[6,29] we observed that the parafoveal circulation compriss three capillary plexuses. Superficial arteries and veins were differentiated after registration of OCT-A with confocal CFP,[25] and vessel hierarchy was classified by using the terms *arteriole* and *venule* based on vessel diameter. However, since with OCT and confocal CFP, small arterioles and venules could not be reliably distinguished from capillaries, we employed the terms *arteriole* and *venule* only for vessels with a diameter $\geq$12 µm and an unequivocal connection to superficial vessels.

Recently, An et al.[15] performed a ground-truth study of macular vasculature analysis using high-resolution confocal microscopy of perfusion-labeled donor eyes. Inflow analysis demonstrated large arteriolar connections from the superficial arteries to the SVC (79%) and to the ICP (21%). The DCP received inflow from small arterioles that connected to arterioles of the ICP. Outflow analysis demonstrated that all three plexuses drain to large venules that connect directly to the venous system and were organized in seven different patterns. While our study corroborates those observations, we add additional information that may be useful for a better understanding of macular blood flow.

We observed that the ratio of inflow patterns (i.e., four arterioles supplying the SVC to one arteriole supplying the ICP) was remarkably constant in the perifovea and that DCP arteriolar inflow follows a distinct spiral shape. Regarding outflow, we characterized outflow patterns according to the venule connecting to the superficial vein. The most prevalent pattern was drainage through SVC venules. This pattern could be further subclassified for the presence of biconvergence (ICP and SVC) or triconvergence (DCP, ICP, and SVC) of draining venules, as previously described in histology.[5,15] The second most common pattern was DVC venules with convergence of ICP and DCP drainage. Other drainage patterns, while observed, were much less prevalent. We also noticed two patterns of capillaries convergence into draining venules at the ICP plane: convergence of two capillaries was the most common pattern (80%), while convergence of three or more capillaries was observed in the remaining cases. These findings agree with the patterns described by An et al.[15] and highlights the role of superficial venules and convergence of venules in macular drainage.

To the best of our knowledge, this is the first study to compared cross-sectional structural OCT features with volume rendering of the macular vascular network to evaluate interplexus connecting vessels. We found that DCP draining venules were the largest connecting vessels crossing the INL and angled toward the target superficial vein. The DCP draining venules have been associated with the pathophysiology of diverse macular vascular disorders, including acute macular neuroretinopathy,[30] exudative nonneovascular age-related macular degeneration,[31] and branch retinal vein occlusion (RVO).[13] In eyes with RVO, the sequalae of ischemia and vascular remodeling have been used to explore blood flow circuitry within the retina. Recently, Iovino et al.[30] published a series of RVO eyes in which there was antecedent DCP ischemia or concurrent with ICP territory ischemia. This observation agrees with early observations, corroborated by our current study, of a series arrangement of DCP inflow through the ICP, making it more prone to ischemic damage in the setting of prolonged arteriovenous transit time and increased pressure in the outflow system.[11,13,15] Another clinically relevant setting is the formation of venous collaterals following branch RVO. Previous studies in humans[13,32] and animals[33] showed that collateral vessels develop preferentially in the DVC. In this work, we observed that arteriolar inflow from superficial arteries is more common to the SVC versus the DVC. Therefore, pressure and flow speed in the SVC would be higher than in the DVC,[34,35] making the latter more prone to collateral formation. However, we acknowledge that a flow-driven explanation is likely incomplete, and other hypotheses should be considered. Histologic studies demonstrated that factors intrinsic to the wall of DCP vessels make them inherently more distensible,[15] while connectivity studies, using the shortest-pathway analysis, demonstrated that connections through the DVC are shortest.[28]

As our observations also apply to commercial SD and swept-source OCT acquisitions with adequate signal-to-noise ratio at the INL plane, they enable a

reappraisal of DCP draining venules in these pathologies. Another practical implication of this observation would be using the spatial association between draining venules and superficial veins to identify veins in structural OCT acquisitions, as previously done in OCT-A using vortex vein analysis.[21]

Strengths of our study include the use of HighRes OCT technology with a 3-µm axial resolution, a 6-µm interscan distance, and a high signal-to-noise ratio. Image analysis followed an innovative strategy, enabling the evaluation of DVC connectivity without the projection artifact limitations of OCT-A technology. The algorithm employed demonstrated a high accuracy and can be applied in future studies. Another major strength is related to segmentation using a semiautomated approach that uses volumetric signal strength.

We acknowledge limitations of our analysis, some of which can be addressed as research questions in future studies. We did not evaluate nasal areas, which might be vascularized by cilioretinal arteries and where the RPCP constitutes a large volume fraction of the SVC. We believe that a future study investigating vascular connectivity in the peripapillary area would be very interesting. As our analysis was limited to a limited number of healthy participants, we could not make inferences regarding its commercial usage or applicability in pathologic states. While HighRes OCT and OCT-A provide enhanced axial resolution, lateral resolution is equal to the commercially available SPECTRALIS platform. Future OCT technology with improved lateral resolution will help refine details of the smaller interplexus connecting vessels.

In summary, methods combining data from dense volumes of highly averaged structural HighRes OCT B-scans with HighRes OCT angiography demonstrate macular vascular connectivity that is more consistent with findings from confocal microscopy than analyses limited to flow-based data. DVC vascular connectivity patterns derived from in vivo HighRes OCT closely matched the vascular patterns observed with high-resolution ex vivo confocal microscopy. In vivo analysis of the macular vasculature supports a hybrid arrangement of blood flow within the human perifoveal macula, with an in-series arrangement between the SVC and DVC.

Acknowledgments

The authors thank Michel Teussink and Sophie Caujolle (Heidelberg Engineering GmbH Germany) for providing technical specifications for the Spectralis HighRes OCT technology. The authors also thank Fernando Vilhena for designing Figure 5.

Supported by the Macula Foundation, Inc. (New York, NY, USA) and by Fundação para a Ciência e Tecnologia (FCT)–Portugal, cofunded by FEDER under the PT2020 Partnership Agreement (to MCS, including project PTDC/MED-PAT/30385/2017, iNOVA4Health-UIDB/04462/2020). ACF was funded by a FCT PhD studentship (PD/BD/135503/2018). DC was supported in part by a studentship from Fundação Luso-Americana para o Desenvolvimento (FLAD, USA R&D@PhD–Proj 2020/0140).

Disclosure: **D. Cabral**, None; **A.C. Fradinho**, None; **T. Pereira**, None; **M.S. Ramakrishnan**, None; **T. Bacci**, None; **D. An**, None; **S. Tenreiro**, None; **M.C. Seabra**, None; **C. Balaratnasingam**, None; **K.B. Freund**, Genentech (C), Optovue (C), Zeiss (C), Heidelberg Engineering (C), Allergan (C), Bayer (C), Novartis (C)

References

1. Hayreh SS. Acute retinal arterial occlusive disorders. *Prog Retin Eye Res*. 2011;30(5):359–394.
2. Tan PEZ, Yu PK, Balaratnasingam C, et al. Quantitative confocal imaging of the retinal microvasculature in the human retina. *Invest Ophthalmol Vis Sci*. 2012;53(9):5728–5736.
3. Henkind P. Radial peripapillary capillaries of the retina. I. Anatomy: human and comparative. *Br J Ophthalmol*. 1967;51(2):115–123.
4. Foreman DM, Bagley S, Moore J, Ireland GW, McLeod D, Boulton ME. Three dimensional analysis of the retinal vasculature using immunofluorescent staining and confocal laser scanning microscopy. *Br J Ophthalmol*. 1996;80(3):246–251.
5. Snodderly DM, Weinhaus RS, Choi JC. Neural-vascular relationships in central retina of macaque monkeys (*Macaca fascicularis*). *J Neurosci*. 1992;12(4):1169–1193.
6. Campbell JP, Zhang M, Hwang TS, et al. Detailed vascular anatomy of the human retina by projection-resolved optical coherence tomography angiography. *Sci Rep*. 2017;7(42201):1–11.
7. Fouquet S, Vacca O, Sennlaub F, Paques M. The 3D retinal capillary circulation in pigs reveals a predominant serial organization. *Invest Ophthalmol Vis Sci*. 2017;58(13):5754–5763.
8. Pi S, Camino A, Wei X, et al. Rodent retinal circulation organization and oxygen metabolism

revealed by visible-light optical coherence tomography. *Biomed Optics Express*. 2018;9(11): 5851.
9. Paques M, Tadayoni R, Sercombe R, et al. Structural and hemodynamic analysis of the mouse retinal microcirculation. *Invest Ophthalmol Vis Sci*. 2003;44(11):4960–4967.
10. Nesper PL, Lee HE, Fayed AE, Schwartz GW, Yu F, Fawzi AA. Hemodynamic response of the three macular capillary plexuses in dark adaptation and flicker stimulation using optical coherence tomography angiography. *Invest Ophthalmol Vis Sci*. 2019;60(2):694–703.
11. Garrity ST, Paques M, Gaudric A, Bailey FK, Sarraf D. Considerations in the understanding of venous outflow in the retinal capillary plexus. *Retina*. 2017;37(10):1809–1812.
12. Ghasemi Falavarjani K, Phasukkijwatana N, Freund KB, et al. En face optical coherence tomography analysis to assess the spectrum of perivenular ischemia and paracentral acute middle maculopathy in retinal vein occlusion. *Am J Ophthalmol*. 2017;177:131–138.
13. Freund KB, Sarraf D, Leong BCS, Garrity ST, Vupparaboina KK, Dansingani KK. Association of optical coherence tomography angiography of collaterals in retinal vein occlusion with major venous outflow through the deep vascular complex. *JAMA Ophthalmol*. 2018;136(11):1262–1270.
14. Tan PEZ, Yu PK, Balaratnasingam C, et al. Quantitative confocal imaging of the retinal microvasculature in the human retina. *Invest Ophthalmol Vis Sci*. 2012;53(9):5728–5736.
15. An D, Yu P, Freund KB, Dao-Yi Y, Balaratnasingam C. Three-dimensional characterization of the normal human parafoveal microvasculature using structural criteria and high-resolution confocal microscopy. *Invest Ophthalmol Vis Sci*. 2020;61(10):3.
16. Spaide RF, Caujolle S, Otto T. Intermediate and deep capillary plexuses in machine learning segmentation of high-resolution optical coherence tomography imaging. *Retina*. 2021;41:1314–1317.
17. Gattoussi S, Freund KB. Correlating structural and angiographic optical coherence tomography in the intermediate and deep retinal capillary plexuses. *Exp Eye Res*. 2017;165:96–98.
18. Izatt JA, Choma MA. Theory of optical coherence tomography. In: Drexler W, Fujimoto JG, eds. *Optical Coherence Tomography*. Berlin, Heidelberg: Springer; 2008:47–72.
19. Zhang M, Hwang TS, Campbell JP, et al. Projection-resolved optical coherence tomographic angiography. *Biomed Optics Express*. 2016; 7(3):816.
20. Campbell R. Kalman filter for noisy movies. MATLAB Central File Exchange (http://www.mathworks.com/matlabcentral/fileexchange/26334-kalman-filter-for-noisy-movies), Retrieved July 10, 2021.
21. Girard MJA, Strouthidis NG, Ross Ethier C, Mari JM. Shadow removal and contrast enhancement in optical coherence tomography images of the human optic nerve head. *Invest Ophthalmol Vis Sci*. 2011;52(10):7738–7748.
22. Mäkinen Y, Azzari L, Foi A. Collaborative filtering of correlated noise: exact transform-domain variance for improved shrinkage and patch matching. *IEEE Trans Image Process*. 2020;9:8339–8354.
23. Spaide RF, Curcio CA. Evaluation of segmentation of the superficial and deep vascular layers of the retina by optical coherence tomography angiography instruments in normal eyes. *JAMA Ophthalmol*. 2017;135(3):259–262.
24. Schindelin J, Arganda-Carreras I, Frise E, et al. Fiji: an open-source platform for biological-image analysis. *Nat Methods*. 2012;9(7):676–682.
25. Xu X, Yannuzzi NA, Fernández-Avellaneda P, et al. Differentiating veins from arteries on optical coherence tomography angiography by identifying deep capillary plexus vortices. *Am J Ophthalmol*. 2019;207:363–372.
26. Hogan MJ, Feeney L. The ultrastructure of the retinal blood vessels. I. The large vessels. *J Ultrastruct Res*. 1963;39:10–28.
27. Hogan MJ, Feeney L. The ultrastructure of the retinal vessels. II. The small vessels. *J Ultrastruct Res*. 1963;49:29–46.
28. Cabral D, Pereira T, Ledesma-Gil G, et al. Volume rendering of dense B-scan optical coherence tomography angiography to evaluate the connectivity of macular blood flow. *Invest Ophthalmol Vis Sci*. 2020;61(6):44.
29. Nesper PL, Fawzi AA. Human parafoveal capillary vascular anatomy and connectivity revealed by optical coherence tomography angiography. *Invest Ophthalmol Vis Sci*. 2018;59(10):3858–3867.
30. Iovino C, Au A, Ramtohul P, et al. Coincident PAMM and AMN and insights into a common pathophysiology. *Am J Ophthalmol*. 2022;236:136–146.
31. Bacci T, Essilfie JO, Leong BCS, Freund KB. Exudative non-neovascular age-related macular degeneration. *Graefes Arch Clin Exp Ophthalmol*. 2021;259(5):1123–1134.

32. Henkind P, Wise GN. Retinal neovascularization, collaterals, and vascular shunts. *Br J Ophthalmol.* 1974;58(4):413–422.
33. Genevois O, Paques M, Simonutti M, et al. Microvascular remodeling after occlusion-recanalization of a branch retinal vein in rats. *Invest Ophthalmol Vis Sci*. 2004;45(2):594–600.
34. Pries AR, Secomb TW, Gaehtgens P. Biophysical aspects of blood flow in the microvasculature. *Cardiovasc Res*. 1996;32(4):654–667.
35. Sirs JA. The flow of human blood through capillary tubes. *J Physiol.* 1994;44(1):569–583.